Topology Optimization for Magnetic Circuits with Continuous Adjoint Method in 3D

Zakaria Houta, Frédéric Messine, Thomas Huguet

Topology Optimization for Magnetic Circuits with Continuous Adjoint Method in 3D

November 12, 2024

Abstract

- Purpose: The aim of this article is to present a new approach to optimizing the design of 3D magnetic circuits. This approach is based on topology optimization, where derivative calculations are performed using the continuous adjoint method. Thus, the continuous adjoint method for magnetostatics has to be developed in 3D and has to be combined with penalization, filtering and homotopy approaches in order to provide an efficient optimization code.
- Design/methodology/approach: In order to provide this new topology optimization code, we start from 2D-magnetostatic results to perform the sensitivity analysis, and this approach is extended to 3D. From this sensitivity analysis, the continuous adjoint method is derived to compute the gradient of an objective function of a 3D topological optimization design problem. From this result, this design problem is discretized and can then be solved by finite element software. Thus, by adding the Solid Isotropic Material with Penalization (SIMP) penalization approach and developing a homotopy-based optimization algorithm, we provide an interesting means for designing 3D magnetic circuits.
- Findings: In this paper, we present the 3D continuous adjoint method for magnetostatic problems involving an objective least-squares function. Based on 2D results, we provide new theoretical results for developing sensitivity analysis in 3D taking into account different parameters including the ferromagnetic material, the current density and the magnetization. Then, by discretizing, filtering and penalizing using SIMP approaches, a topology optimization code has been derived to address only the ferromagnetic material parameters. Based on this efficient gradient computation method, we develop a homotopy-based optimization algorithm for solving large-scale 3D design problems.
- Originality/value: In this paper, we propose an approach based on topology optimization to solve 3D magnetostatic design problems when an objective least-squares function is involved. This approach is based on the continuous adjoint method we have derived for 3D magnetostatic design problems. The effectiveness of this topology optimization code is demonstrated by solving the design of a 3D magnetic circuit with up to 100,000 design variables.

Keywords: Topology Optimization, Adjoint Method, Sensitivity Analysis, Magnetostatic Inverse Problem.

1 Introduction

Topology optimization was first introduced to design 2D mechanical structures, (Allaire 2007, Bendsøe & Sigmund 2003, Sigmund 2007); as for example, to design the inside mechanical

structures of airplane wings, (Aage, Andreassen, Lazarov & Sigmund 2017). Among different topology optimization approaches, the main interesting ones for solving large problems, are based on continuous relaxations of the binary variables which are used to show whether a cell is air or material. Thus, local descent based algorithms can be efficiently used to solve these large-scale problems. During the optimization process, the intermediate points have to be penalized in order to enforce local optimization solvers to converge to binary solutions representing for example air or material. Bendsoe et al. have introduced the well-known *Solid Isotropic Material with Penalization* (SIMP) approach and various penalization schemes can be found in (Bendsøe & Sigmund 2003, Bendsøe & Sigmund 1999, Sanogo & Messine 2018, Gauthey, Gangl & Hassan 2021). It is worth noting that *SIMP*-based methods are widely used in professional solvers, as for example `OptiStruct` of *Altair company*. Because local search solvers are based on gradient descent steps, the computations of the derivative has to be very efficient. Thus *adjoint methods* were developed to provide the gradient of a function which depends on expensive computations based numerical simulations, (Allaire 2007, Bendsøe & Sigmund 2003, Sigmund 2007).

More recently, new codes were implemented to solve 3D design problems in mechanics mainly based on voxels (boxes which are extensions of the 2D-pixel). The most famous result was obtained by Aage et al. in (Aage et al. 2017) who designed a 3D airplane wing for Boeing with a billion of voxels. This result was obtained in 5 days using a parallel code based on *SIMP*, adjoint method and a local search algorithm.

From approaches in mechanics, some studies were done to solve topology optimization design problems in electromagnetism dealing with Maxwell equations. Specially in magnetostatics, to solve these kinds of problems, the adjoint method has also been developed, (Sanogo, Messine, Henaux & Vilamot 2014, Youness & Messine 2019*b*, Gauthey et al. 2021, Gauthey, Hassan, Messine & Gillon 2023). In (Sanogo 2016), magnetic circuits were designed in such a way. More recently the nonlinearity of ferromagnetic material has been taken into account in (Youness & Messine 2019*a*) and (Gauthey et al. 2021). Moreover, some new material schemes also called penalization schemes were introduced for this *SIMP* method dedicated to problems in magnetostatics, (Sanogo & Messine 2018, Gauthey et al. 2021). A recent survey paper present and discuss about all the conventional approaches developed in order to solve topology optimization design problems in electromagnetism, (Lucchini, Torchio, Cirimele, Alotto & Paolo 2022). This paper emphasizes on the intrinsic advantages and limits of all these approaches, (Lucchini et al. 2022).

As far as we know, topology optimization using continuous adjoint methods in magnetostatics has only been developed for 2D design problems. Nevertheless, note that in (Seebacher, Kaltenbacher, Wein & Lehmann 2021), a first recent study to design 3D-magnetic circuit is done but using a discrete adjoint method associated with SIMP approach. This adjoint method needs to first discretize the problem by a finite element methods and then, the adjoint problem can be quite directly derived. In the continuous approach that we developed in this work, the adjoint method is directly applied to the continuous formulation of the problem and therefore, it is not directly linked to the used discretization numerical method. Some other works deal also with electromagnetic design in 3D but they are based on topological derivative methods which are derived from shape optimization, (Masmoudi, Pommier & Samet 2005, Gangl & Sturm 2021). In this paper, we extend the topology optimization with adjoint method for 3D design problems in magnetostatics with the assumption that the ferromagnetic materials are linear. Note that, this could not be a big issue to extend the 3D-adjoint method including the non-linearity of ferromagnetic materials as it is shown in recent works for the 2D case, (Youness & Messine 2019*a*, Gauthey et al. 2021). Indeed, instead to solve a linear system, we will have to solve a nonlinear one and as shown in (Gauthey et al. 2021), that will multiply by about 7 the total CPU-times. Moreover, another limitation of this paper is that we focus on topology optimization to address design problems of a unique material. This also could be extended following recent works in 2D, (Gauthey et al. 2021, Cherrière, Laurent, Hlioui, Louf, Duysinx, Geuzaine, Ben Ahmed, Gabsi & Fernández 2022).

In Section 2, topology optimization with continuous adjoint method is recalled for 2D design problems in magnetostatics. Section 3 is dedicated to the extension to 3D design problems with a new theoretical formulation of the gradient based on the continuous adjoint method. In Section 4,

we detail our algorithmic approach to solve topology optimization problems using *SIMP* techniques. Section 5 is dedicated to the gradient verification (by comparing it to the finite difference technique) and to numerical tests to design a 3D magnetic circuit. Section 6 concludes.

2 Problem description

In this work, Ω represents the whole studied domain. Within Ω, Ω_V represents the variable domain in which the matter can be added or removed. This matter can be permanent magnet in $\Omega_V(\mathbf{M})$, coils with current in $\Omega_V(\mathbf{J})$ or ferromagnetic material in $\Omega_V(\nu_r)$. Ω_T represents the target domain in which a particular magnetic flux density $\mathbf{B}_0$ has to be imposed playing with the matter in Ω_V. In this work $\Omega_V(\mathbf{M})$, $\Omega_V(\mathbf{J})$ and $\Omega_V(\nu_r)$ have to be disconnected.

The topology optimization problem is defined as follows:

- The *objective function* is the squared error in a target zone Ω_T between an imposed magnetic flux density $\mathbf{B}_0$ and the magnetic flux density $\mathbf{B}$ obtained with respect to the magnetic sources and the material distributions in all the domain Ω. Note that $\mathbf{B}$ has to be computed by solving Maxwell magnetostatic equations.
- The *design variables* are magnetic sources (active material) such as ferromagnetic material, coil with current density and permanent magnets. The associated variables for all the variable domains Ω_V are the distribution of relative reluctivity ν_r, current density $\mathbf{J}$ (in the 3 directions (x, y, z)) and magnetization $\mathbf{M}$ (in the 3 directions (x, y, z)). Hence, we define a global variable $\mathbf{p}$ as:

$$\mathbf{p} : \left| \begin{array}{rcl} \Omega_V & \longrightarrow & \mathbb{R}^7 \\ (x,y,z)^T & \longmapsto & \mathbf{p}(x,y,z) = (p_1, \cdots, p_7)^T \end{array} \right.$$

  Where $\mathbf{p} = (\nu_r, J_x, J_y, J_z, M_x, M_y, M_z)^T$ and we define the three following functions: $\nu_r(\mathbf{p}) = \nu_r$, $\mathbf{J}(\mathbf{p}) = (J_x, J_y, J_z)^T$ and $\mathbf{M}(\mathbf{p}) = (M_x, M_y, M_z)^T$.

Note that, $\mathbf{p}$ is defined in the whole domain Ω, $\mathbf{p}$ is fixed on $\Omega \setminus \Omega_V$ and is variable on Ω_V.

Therefore, the optimization problem that we addressed, is the following:

$$\min_{\mathbf{p}} F_o(\mathbf{p}) = \int_{\Omega_T} || \mathbf{B}(\mathbf{A}(\mathbf{p})) - \mathbf{B}_0 ||^2 \, d\Omega, \tag{1}$$

where $\mathbf{A}$ corresponds to the magnetic potential vector obtained by solving the Maxwell equations.

In this work, the constitutive law of the magnetic materials is supposed to be linear in order to simplify the computations in 3D; some extensions to the non-linear case can be done from (Gauthey et al. 2021) and (Youness & Messine 2019*a*).

Hence, considering the linear case, we have:

$$\mathbf{H} = \nu \mathbf{B} - \mathbf{M} \tag{2}$$

Where $\nu = \nu_0 \nu_r$ is the magnetic reluctivity of the material, ν_0 is the air reluctivity and ν_r is the relative reluctivity of the material.

In different points of domain Ω, we have for $\mathbf{p}$:

- For air: $\nu_r = 1$, $\mathbf{M} = \mathbf{0}$ and $\mathbf{J} = \mathbf{0}$ in the 3 directions.
- For ferromagnetic material: ν_r is a constant depending on the material (in this paper, $\nu_r = \frac{1}{1000}$), $\mathbf{M} = \mathbf{0}$ and $\mathbf{J} = \mathbf{0}$ in the 3 directions.
- For permanent magnets: $\nu_r = 1$, $\mathbf{M}$ is a constant bounded vector in 3D and $\mathbf{J} = \mathbf{0}$ in the 3 directions.
- For coils: $\nu_r = 1$, $\mathbf{M} = \mathbf{0}$ and $\mathbf{J}$ is a constant bounded vector in 3D.

Because $\mathbf{p}$ is extended on the whole domain Ω, in $\Omega \setminus \Omega_V$ (with $\Omega_V = \Omega_V(\nu_r) \cup \Omega_V(\mathbf{M}) \cup \Omega_V(\mathbf{J})$), $\mathbf{p}$ is fixed and cannot change during the optimization process. Thus, in $\Omega \setminus \Omega_V$, $\mathbf{p}$ can be air, a ferromagnetic material, a permanent magnet or a coil. In the variable domain Ω_V, $\mathbf{p}$ is variable and can be air or a ferromagnetic material if $(x, y, z)^T$ belongs to $\Omega_V(\nu_r)$, air or a permanent magnet if $(x, y, z)^T$ belongs to $\Omega_V(\mathbf{M})$ and air or a coil if $(x, y, z)^T$ belongs to $\Omega_V(\mathbf{J})$.

The Maxwell-Ampere equation $\nabla \times \mathbf{H} = \mathbf{J}$ becomes, using the constitutive law of the material described in equation (2) and the existence of the potential vector $\mathbf{A}$ such that $\mathbf{B} = \nabla \times \mathbf{A}$:

$$-\nabla \times [\nu_0 \nu_r(\mathbf{p}) \mathbf{B}(\mathbf{A}(\mathbf{p})) - \mathbf{M}(\mathbf{p})] + \mathbf{J}(\mathbf{p}) = 0, \text{in } \Omega. \tag{3}$$

Equation (3) is called, in this paper, the primal problem. Note that $\mathbf{B}(.)$ is the curl operator $\nabla \times (.)$ which is also denoted by $\mathbf{B}(\mathbf{A}) = \mathbf{curl}(\mathbf{A})$. The Dirichlet condition $\mathbf{A} \times \mathbf{n} = \mathbf{0}$ is imposed on the domain boundary $\partial\Omega$, where $\mathbf{n}$ is the normal vector (this hypothesis is relevant because the border of the domain Ω is far from the zone of interest Ω_T).

The partial derivative $\frac{\partial F_o}{\partial p_i}$ is calculated using the adjoint method. Hence, from equations (1) and (3), the optimization problem (1) can be equivalently formulated as:

$$(\mathcal{P}) \begin{cases} \min\limits_{\mathbf{p},\mathbf{A}} & F(\mathbf{p}, \mathbf{A}) = \int_{\Omega_T} || \mathbf{B}(\mathbf{A}) - \mathbf{B}_0 ||^2 \, d\Omega \\ uc & \\ & -\nabla \times [\nu_0 \nu_r(\mathbf{p}) \mathbf{B}(\mathbf{A}) - \mathbf{M}(\mathbf{p})] + \mathbf{J}(\mathbf{p}) = 0 \text{ in } \Omega, \\ & \text{with} \quad \mathbf{A} \times \mathbf{n} = 0 \text{ in } \partial\Omega \\ & \mathbf{p} \in \mathscr{P} := \{\mathbf{p} \in (L^\infty(\Omega))^7 : p_i^{\min} \leq p_i \leq p_i^{\max}, i = 1, \cdots, 7\} \end{cases} \tag{4}$$

Where $\mathbf{p}^{\min}$ and $\mathbf{p}^{\max}$ are the lower and upper bounds of the variable $\mathbf{p}$. Note that in $(\mathcal{P})$, the variables $\mathbf{p}$ and $\mathbf{A}$ are separated and linked by the constraint which is the Maxwell equation. Moreover if $\mathbf{p}$ satisfies the Maxwell constraint, then $F_o(\mathbf{p}) = F(\mathbf{p}, \mathbf{A})$ and therefore, for such a point $\mathbf{p}$:

$$\frac{\partial F_o}{\partial p_i}(\mathbf{p}) = \frac{\partial F}{\partial p_i}(\mathbf{p}, \mathbf{A}).$$

3 Sensitivity analysis from 2D to 3D

Efficient optimization codes are based on computations of the derivatives. These derivatives can be obtained with evaluations of the objective function considering small variations of the variable $\mathbf{p}$. This defines the well-known finite difference method. However, all these evaluations require to solve Maxwell equations using a numerical solver. Hence, because it depends directly to the number of variables, the finite difference technique is extremely expensive.

Thus, adjoint methods has been developed in order to compute the derivatives with more efficiency. It was first developed in mechanics (Allaire 2007, Bendsøe & Sigmund 2003), then extended to 2D magnetostatics (Sanogo 2016, Sanogo et al. 2014) and to 2D electrical machines (Gauthey et al. 2021, Cherrière et al. 2022).

Thus, in the first subsection 3.1, the 2D magnetosatic continuous adjoint method is recalled. In the following subsection 3.2, the continuous adjoint method is extended to the 3D-case.

3.1 Sensitivity analysis in 2D

Generally, due to symmetries and invariances along one direction, 3D magnetostatic problems can be simplified in 2D problems.

Considering the Cartesian coordinates in 3D: (x, y, z) and an invariance following z, the magnetic flux density can be reduced to $\mathbf{B} = (B_x, B_y)^T$. Furthermore:

- The potential vector is a scalar:

$$\mathbf{A} = (0, 0, A(x, y)) \equiv A(x, y)$$

- The magnetic density flux is a 2D vector:

$$\mathbf{B}(A) = \mathbf{curl}(\mathbf{A}) = (\partial_y A, -\partial_x A, 0) \equiv (\partial_y A, -\partial_x A)$$

- The boundary condition is reduced to $A = 0$ on the boundary domain $\partial\Omega$.

In order to solve problem $(\mathcal{P})$, it is necessary to compute the derivative of the function F_o with respect to the design variable $\mathbf{p}$. The sensitivity calculation in 2D is summarized below (for more details see (Sanogo 2016) and (Sanogo et al. 2014)):

- For problem $(\mathcal{P})$, the Lagrangian function $\mathscr{L}$ is introduced as follows:

$$\mathscr{L}(\mathbf{p}, A, \lambda) = F(\mathbf{p}, A) + \int_\Omega \lambda\mu_0 \left[-\nabla \times (\nu_0\nu_r(\mathbf{p})\mathbf{B}(A) - \mathbf{M}(\mathbf{p})) + J(\mathbf{p})\right] d\Omega,$$

  where the equality constraint is multiplied by the Lagrangian multiplier λ which is a scalar function. λ belongs to $H_0^1(\Omega)$ (a standard Sobolev space) with the same properties as A. Note that, the equality constraint of $(\mathcal{P})$ is also multiplied by μ_0 (the void permeability $= \frac{1}{\nu_0}$) in order to ensure the homogeneity considering the physical units in the summed terms. Note that this Lagrangian formulation is in 2D, with A a scalar function, $\mathbf{M}$ a vector (in 2D), J is also a scalar (in direction z) and the curl operator in 2D is scalar $\nabla \times (v_x, v_y)^T = \partial_x v_y - \partial_y v_x$.

- Using the Green formula in 2D, we obtain:

$$\frac{\partial \mathbf{B}}{\partial A}(A) = \mathbf{B}(.),$$

  and the continuous adjoint problem in 2D is:

$$\nabla \times [\nu\mathbf{B}(\lambda) - \mathbf{M}_a \mathbb{1}_{\Omega_T}] = 0, \text{in } \Omega, \tag{5}$$

  with $\mathbb{1}_{\Omega_T}$ is the indicator function, defined by:

$$\mathbb{1}_{\Omega_T}(x) = \begin{cases} 1 & \text{if } x \in \Omega_T \\ 0 & \text{if } x \in \Omega \setminus \Omega_T \end{cases}$$

  where λ is named the adjoint variable and $\mathbf{M}_a = \frac{2}{\mu_0}(B_x - B_{0x}, B_y - B_{0y})^T$ can be understood as a permanent magnet in Ω_T. This adjoint problem is therefore equivalent to a magnetostatic problem with only one source $\mathbf{M}_a$.

  Note that, the computation of $\mathbf{M}_a$ depends on the value of the field $\mathbf{B} = (B_x, B_y)^T$ in Ω_T which must be previously calculated by solving the primal problem defined by equation (3).

- From the equality $\frac{\partial F_o(\mathbf{p})}{\partial \mathrm{p}_i} = \frac{\partial \mathscr{L}}{\partial \mathrm{p}_i}(\mathbf{p}, A(\mathbf{p}), \lambda)$ which is verified for any couple $(\mathbf{p}, A)$ satisfying the constraint (3), the sensitivity formula is obtained by deriving the Lagrangien $\mathscr{L}$ with respect to the design variable $\mathbf{p}$:

$$\frac{\partial F_o(\mathbf{p})}{\partial \mathrm{p}_i} = \int_\Omega \mu_0 \big[\lambda \frac{\partial J(\mathbf{p})}{\partial \mathrm{p}_i} + \mathbf{B}(\lambda).\frac{\partial \mathbf{M}(\mathbf{p})}{\partial \mathrm{p}_i} - \nu_0 \frac{\partial \nu_r(\mathbf{p})}{\partial \mathrm{p}_i}\mathbf{B}(\lambda).\mathbf{B}(A)\big] d\Omega, \tag{6}$$

  for each component p_i of $\mathbf{p}$; only $p_1 = \nu_r, p_4 = J_z, p_5 = M_x$ and $p_6 = M_y$ are used in this 2D problem.

  Note that in the sensitivity formula (6), A and λ are solutions of equations (3) and (5), respectively.

Equations (3) and (5) can be solved by the finite element method whose weak formulation is written as:

$$\int_\Omega \nu\mathbf{B}(X).\mathbf{B}(\phi)d\Omega - \int_\Omega \mathbf{M}.\mathbf{B}(\phi)d\Omega - \int_\Omega J\phi d\Omega = 0, \tag{7}$$

where ϕ is a test function of $H_0^1(\Omega)$.

For example, in order to solve the primal problem of designing a simple magnetic circuit with only a coil, a ferromagnetic material and no permanent magnet, we just have to take $X = A$, $\mathbf{M} = \mathbf{0}$ and the only source is the current J. Considering the same example, the adjoint problem is derived from equation (7) by taking $X = \lambda$, $J = 0$ and the only source is $\mathbf{M} = \mathbf{M}_a$.

In a 2D problem, equation (7) can be simplified, such as:

$$\int_\Omega \nu \nabla X.\nabla \phi \, d\Omega - \int_\Omega \begin{pmatrix} -M_y \\ M_x \end{pmatrix} .\nabla \phi \, d\Omega - \int_\Omega J\phi \, d\Omega = 0, \forall \phi \in H_0^1(\Omega). \tag{8}$$

3.2 Sensitivity analysis and continuous adjoint method in 3D

In this subsection, we detail the steps to compute the sensitivity of the objective function F_o with respect to the design variable p_i for a 3D problem. Note that in 3D, the potential vector and the magnetic flux density have non zero-components, and then,

- The potential vector is:

$$\mathbf{A} = (A_x(x, y, z), A_y(x, y, z), A_z(x, y, z))$$

- The magnetic flux density is:

$$\mathbf{B}(\mathbf{A}) = \mathbf{curl}(\mathbf{A}) = (\partial_y A_z - \partial_z A_y, \partial_z A_x - \partial_x A_z, \partial_x A_y - \partial_y A_x)^T$$

- The boundary condition is $\mathbf{A} \times \mathbf{n} = \mathbf{0}$ on the boundary domain $\partial\Omega$.

The following theorem is dedicated to the computations in 3D of the partial derivatives of the original function F_o.

Theorem 1. *The expression in 3D of the sensitivity of F_o with respect to each component p_i of $\boldsymbol{p}$ is:*

$$\frac{\partial F_o(\boldsymbol{p})}{\partial p_i} = \int_\Omega \mu_0 \left(\boldsymbol{\lambda}.\frac{\partial \boldsymbol{J}(\boldsymbol{p})}{\partial p_i} + \boldsymbol{B}(\boldsymbol{\lambda}).\frac{\partial \boldsymbol{M}(\boldsymbol{p})}{\partial p_i} - \nu_0 \frac{\partial \nu_r(\boldsymbol{p})}{\partial p_i} \boldsymbol{B}(\boldsymbol{\lambda}).\boldsymbol{B}(\boldsymbol{A}) \right) d\Omega, \tag{9}$$

where $\boldsymbol{B}(\boldsymbol{\lambda})$ is obtained by solving the following continuous adjoint problem:

$$\nabla \times [\boldsymbol{M}_a \mathbb{1}_{\Omega_T} - \nu \boldsymbol{B}(\boldsymbol{\lambda})] = 0, \tag{10}$$

with $\boldsymbol{M}_a$ which is the adjoint magnetization defined as follows:

$$\boldsymbol{M}_a = \frac{2}{\mu_0} \begin{pmatrix} B_x - B_{0x} \\ B_y - B_{0y} \\ B_z - B_{0z} \end{pmatrix},$$

with $\boldsymbol{B} = (B_x, B_y, B_z)^T$ which is the magnetic flux density.

Note that equation (10) is the adjoint problem in 3D. It is equivalent to a magnetostatic problem where $\mathbf{M}_a$ is the only source. This problem has to be solved numericaly in order to provide $\boldsymbol{\lambda}$ and $\mathbf{B}(\boldsymbol{\lambda})$.

Proof. The proof of Theorem 1 is based on the following 3 steps:

1. Construction of the Lagrangian function by considering the formulation of problem $(\mathcal{P})$.
2. Determination of the continuous adjoint problem from the Karush-Khun-Tucker theorem.
3. Computation of the topological sensitivity.

Note that, in 3D, we work in the following Sobolev spaces:

$$\mathbf{H}(\mathbf{curl},\Omega)=\left\{\mathbf{w}\in\mathbf{L}^2(\Omega),\mathbf{curl}(\mathbf{w})\in\mathbf{L}^2(\Omega)\right\},$$

$$\mathbf{H}_0(\mathbf{curl},\Omega)=\left\{\mathbf{w}\in\mathbf{H}(\mathbf{curl},\Omega),\text{with }\mathbf{w}\times\mathbf{n}=\mathbf{0}\text{ in }\partial\Omega\right\},$$

because we will need to integrate the vectors $\mathbf{A}$, $\boldsymbol{\lambda}$, $\mathbf{curl}(\mathbf{A})$ and $\mathbf{curl}(\boldsymbol{\lambda})$ in Ω. $\mathbf{L}^\infty(\Omega)$ is the space of bounded vector functions on Ω.

1. **Construction of the Lagrangian function:**
   The Lagrangian function $\mathscr{L}$ is defined as the addition of the objective function and the sum of the equal constraints multiplied by a Lagrange multiplier $\boldsymbol{\lambda}$:

$$\mathscr{L}(\mathbf{p},\mathbf{A},\boldsymbol{\lambda})=F(\mathbf{p},\mathbf{A})+\int_\Omega\boldsymbol{\lambda}.\mu_0\left[-\nabla\times(\nu_0\nu_r(\mathbf{p})\mathbf{B}(\mathbf{A})-\mathbf{M}(\mathbf{p}))+\mathbf{J}(\mathbf{p})\right]d\Omega,$$

   where $(\mathbf{p},\mathbf{A},\boldsymbol{\lambda})\in\mathbf{L}^\infty(\Omega)\times\mathbf{H}_0(\mathbf{curl},\Omega)\times\mathbf{H}_0(\mathbf{curl},\Omega)$ and $\mu_0=\frac{1}{\nu_0}$ the void permeability. The equality constraint of $(\mathcal{P})$ is multiplied by μ_0 (the void permeability $=\frac{1}{\nu_0}$) in order to ensure homogeneity considering the physical units in the summed terms. By using Green formula in 3D:

$$-\int_\Omega\mathbf{v}.(\nabla\times\mathbf{u})d\Omega=-\int_\Omega(\nabla\times\mathbf{v}).\mathbf{u}d\Omega+\int_{\partial\Omega}\mathbf{v}\times\mathbf{n}.\mathbf{u}d\partial\Omega$$

   and by taking: $\mathbf{v}=\mu_0\boldsymbol{\lambda}$ and $\mathbf{u}=\nu\mathbf{B}(\mathbf{A})-\mathbf{M}$, we obtain:

$$\begin{aligned}\int_\Omega\boldsymbol{\lambda}.\mu_0\left[-\nabla\times(\nu\mathbf{B}(\mathbf{A})-\mathbf{M})+\mathbf{J}\right]d\Omega=\quad&\int_\Omega\mu_0\boldsymbol{\lambda}.\mathbf{J}d\Omega\\&-\int_\Omega\mu_0\mathbf{curl}(\boldsymbol{\lambda}).(\nu\mathbf{B}(\mathbf{A})-\mathbf{M})d\Omega\\&+\int_{\partial\Omega}\mu_0(\boldsymbol{\lambda}\times\mathbf{n}).(\nu\mathbf{B}(\mathbf{A})-\mathbf{M})d\partial\Omega.\end{aligned}$$

   Because $\boldsymbol{\lambda}\in\mathbf{H}_0(\mathbf{curl},\Omega),\boldsymbol{\lambda}\times\mathbf{n}=\mathbf{0}$ in $\partial\Omega$, hence we have:

$$\begin{aligned}\int_\Omega\boldsymbol{\lambda}.\mu_0\left[-\nabla\times(\nu\mathbf{B}(\mathbf{A})-\mathbf{M})+\mathbf{J}\right]d\Omega&=\int_\Omega\mu_0\boldsymbol{\lambda}.\mathbf{J}d\Omega-\int_\Omega\mu_0\mathbf{B}(\boldsymbol{\lambda}).(\nu\mathbf{B}(\mathbf{A})-\mathbf{M})d\Omega\\&=\int_\Omega\mu_0\left[\boldsymbol{\lambda}.\mathbf{J}-\nu\mathbf{B}(\boldsymbol{\lambda}).\mathbf{B}(\mathbf{A})+\mathbf{B}(\boldsymbol{\lambda}).\mathbf{M}\right]d\Omega.\end{aligned}$$

   Finally, the Lagrangian function is:

$$\begin{aligned}\mathscr{L}(\mathbf{p},\mathbf{A},\boldsymbol{\lambda})=&\int_{\Omega_T}||\,\mathbf{B}(\mathbf{A})-\mathbf{B}_0\,||^2\,d\Omega\\&+\int_\Omega\mu_0\left[\boldsymbol{\lambda}.\mathbf{J}(\mathbf{p})-\nu(\mathbf{p})\mathbf{B}(\boldsymbol{\lambda}).\mathbf{B}(\mathbf{A})+\mathbf{B}(\boldsymbol{\lambda}).\mathbf{M}(\mathbf{p})\right]d\Omega.\end{aligned}\quad(11)$$

2. **Determination of the continuous adjoint problem:**
   The directional derivative of a function $f:E\to F$ in u in the direction h with $(u,h)\in E^2$ is defined by:

$$D_hf(u)=\lim_{t\to0}\frac{f(u+th)-f(u)}{t}.$$

   If E is an euclidean vector space, and f is a real-valued differentiable application, then we can use the gradient of f to express the directional derivative:

$$D_hf(u)=<\nabla f(u)\mid h>.$$

In order to determine the adjoint system, we use the necessary optimality conditions at the first order of the Karush-Kuhn-Tucker (KKT) theorem. Thus, the directional derivative of $\mathscr{L}$ in $\mathbf{A}$ in any direction $\boldsymbol{\varphi}$ must satisfy:

$$< \frac{\partial \mathscr{L}(\mathbf{p}, \mathbf{A}, \boldsymbol{\lambda})}{\partial \mathbf{A}} \mid \boldsymbol{\varphi} >= 0, \ \forall \boldsymbol{\varphi} \in \mathbf{H}_0(\mathbf{rot}, \Omega). \tag{12}$$

By considering a function f defined by:

$$\mathscr{L}(\mathbf{p}, \mathbf{A}, \boldsymbol{\lambda}) = \int_{\Omega} f(\mathbf{p}, \mathbf{A}, \boldsymbol{\lambda}) d\Omega, \tag{13}$$

where,

$$f(\mathbf{p}, \mathbf{A}, \boldsymbol{\lambda}) = || \ \mathbf{B}(\mathbf{A}) - \mathbf{B}_0 \ ||^2 \ \mathbb{1}_{\Omega_T} + \mu_0 \left[\boldsymbol{\lambda}.\mathbf{J}(\mathbf{p}) - \nu(\mathbf{p}) \mathbf{B}(\boldsymbol{\lambda}).\mathbf{B}(\mathbf{A}) + \mathbf{B}(\boldsymbol{\lambda}).\mathbf{M}(\mathbf{p}) \right].$$

By developing the expression of the Lagrangian (13), and using the linearity property of integrals, we obtain:

$$\begin{aligned}
< \frac{\partial \mathscr{L}(\mathbf{p}, \mathbf{A}, \boldsymbol{\lambda})}{\partial \mathbf{A}} \mid \boldsymbol{\varphi} > &= \lim_{t \to 0} \frac{\mathscr{L}(\mathbf{p}, \mathbf{A} + t\boldsymbol{\varphi}, \boldsymbol{\lambda}) - \mathscr{L}(\mathbf{p}, \mathbf{A}, \boldsymbol{\lambda})}{t} \\
&= \lim_{t \to 0} \frac{\int_{\Omega} f(\mathbf{p}, \mathbf{A} + t\boldsymbol{\varphi}, \boldsymbol{\lambda}) d\Omega - \int_{\Omega} f(\mathbf{p}, \mathbf{A}, \boldsymbol{\lambda}) d\Omega}{t} \\
&= \int_{\Omega} \lim_{t \to 0} \frac{f(\mathbf{p}, \mathbf{A} + t\boldsymbol{\varphi}, \boldsymbol{\lambda}) - f(\mathbf{p}, \mathbf{A}, \boldsymbol{\lambda})}{t} d\Omega \\
&= \int_{\Omega} D_{\boldsymbol{\varphi}} f(\mathbf{A}) d\Omega \\
&= \int_{\Omega} < \nabla_{\mathbf{A}} f \mid \boldsymbol{\varphi} > d\Omega \\
&= \int_{\Omega} \frac{\partial f}{\partial A_x} \varphi_x + \frac{\partial f}{\partial A_y} \varphi_y + \frac{\partial f}{\partial A_z} \varphi_z d\Omega.
\end{aligned}$$

Using the derivation of compound functions, for each of the partial derivatives, where $A_.$ denotes A_x, A_y or A_z, then we have:

$$\begin{aligned}
\frac{\partial f}{\partial A_.} &= \frac{\partial}{\partial A_.} \left[|| \ \mathbf{B}(\mathbf{A}) - \mathbf{B}_0 \ ||^2 \ \mathbb{1}_{\Omega_T} + \mu_0 \left[\boldsymbol{\lambda}.\mathbf{J} - \nu \mathbf{B}(\boldsymbol{\lambda}).\mathbf{B}(\mathbf{A}) + \mathbf{B}(\boldsymbol{\lambda}).\mathbf{M} \right] \right] \\
&= \frac{\partial}{\partial \mathbf{B}(\mathbf{A})} (|| \ \mathbf{B}(\mathbf{A}) - \mathbf{B}_0 \ ||^2 \ \mathbb{1}_{\Omega_T}) . \frac{\partial \mathbf{B}(\mathbf{A})}{\partial A_.} - \mu_0 \nu \mathbf{B}(\boldsymbol{\lambda}) . \frac{\partial \mathbf{B}(\mathbf{A})}{\partial A_.} \\
&= \mathbf{B}_a . \frac{\partial \mathbf{B}(\mathbf{A})}{\partial A_.} \mathbb{1}_{\Omega_T} - \mu_0 \nu \mathbf{B}(\boldsymbol{\lambda}) . \frac{\partial \mathbf{B}(\mathbf{A})}{\partial A_.} \\
&= \left[\mathbf{B}_a \mathbb{1}_{\Omega_T} - \mu_0 \nu \mathbf{B}(\boldsymbol{\lambda}) \right] . \frac{\partial \mathbf{B}(\mathbf{A})}{\partial A_.},
\end{aligned}$$

with:

$$\mathbf{B}_a = 2 \begin{pmatrix} B_x - B_{0x} \\ B_y - B_{0y} \\ B_z - B_{0z} \end{pmatrix}.$$

Thus, we obtain:

$$< \frac{\partial \mathscr{L}(\mathrm{p}, \mathbf{A}, \boldsymbol{\lambda})}{\partial \mathbf{A}} \mid \boldsymbol{\varphi} >= \int_{\Omega} \left[\mathbf{B}_a \mathbb{1}_{\Omega_T} - \mu_0 \nu \mathbf{B}(\boldsymbol{\lambda}) \right] . \left[\varphi_x \frac{\partial \mathbf{B}(\mathbf{A})}{\partial A_x} + \varphi_y \frac{\partial \mathbf{B}(\mathbf{A})}{\partial A_y} + \varphi_z \frac{\partial \mathbf{B}(\mathbf{A})}{\partial A_z} \right] d\Omega. \tag{14}$$

Expanding the term with partial derivatives according to the components of $\mathbf{A}$, we obtain:

$$\left[\varphi_x \frac{\partial \mathbf{B}(\mathbf{A})}{\partial A_x} + \varphi_y \frac{\partial \mathbf{B}(\mathbf{A})}{\partial A_y} + \varphi_z \frac{\partial \mathbf{B}(\mathbf{A})}{\partial A_z}\right] = J_{\mathbf{B}}(\mathbf{A})\boldsymbol{\varphi} \\ = D_{\boldsymbol{\varphi}}\mathbf{B}(\mathbf{A}).$$

Where $J_{\mathbf{B}}(\mathbf{A})$ is the Jacobian matrix of the function $\mathbf{B}$ with respect to $\mathbf{A}$. For each element $\mathbf{A} = (A_x, A_y, A_z)^T \in \mathbb{R}^3$ it is associated $\mathbf{B}(\mathbf{A}) = (B_x(\mathbf{A}), B_y(\mathbf{A}), B_z(\mathbf{A}))^T \in \mathbb{R}^3$.

Using the definition of the directional derivative and the linearity of the **curl** operator, we have:

$$D_{\boldsymbol{\varphi}}\mathbf{B}(\mathbf{A}) = \mathbf{B}(\boldsymbol{\varphi}). \tag{15}$$

From equation (14) and using equation (15), we have:

$$\int_\Omega [\mathbf{B}_a \mathbb{1}_{\Omega_T} - \mu_0 \nu \mathbf{B}(\boldsymbol{\lambda})].\mathbf{B}(\boldsymbol{\varphi}) d\Omega = 0.$$

By applying the Green formula in 3D, we obtain:

$$\int_\Omega \boldsymbol{\varphi}.\nabla \times [\mathbf{B}_a \mathbb{1}_{\Omega_T} - \mu_0 \nu \mathbf{B}(\boldsymbol{\lambda})] d\Omega + \int_{\partial\Omega} (\boldsymbol{\varphi} \times \mathbf{n}).[\mathbf{B}_a \mathbb{1}_{\Omega_T} - \mu_0 \nu \mathbf{B}(\boldsymbol{\lambda})] d\partial\Omega = 0. \tag{16}$$

Because $\boldsymbol{\varphi} \in \mathbf{H}_0(\mathbf{curl}, \Omega), \boldsymbol{\varphi} \times \mathbf{n} = \mathbf{0}$ on $\partial\Omega$, we have:

$$\int_\Omega \boldsymbol{\varphi}.\nabla \times [\mathbf{B}_a \mathbb{1}_{\Omega_T} - \mu_0 \nu \mathbf{B}(\boldsymbol{\lambda})] d\Omega = 0, \quad \forall \boldsymbol{\varphi} \in \mathbf{H}_0(\mathbf{rot}, \Omega).$$

Using Corollary 2.2.2 in (Allaire & Alouges 2015) on elements of $\mathbf{L}^2(\Omega)$:

$$\nabla \times [\mathbf{B}_a \mathbb{1}_{\Omega_T} - \mu_0 \nu \mathbf{B}(\boldsymbol{\lambda})] = 0.$$

By multiplying the above equation by $\frac{1}{\mu_0}$, we find the following expression of the adjoint problem:

$$\nabla \times [\mathbf{M}_a \mathbb{1}_{\Omega_T} - \nu \mathbf{B}(\boldsymbol{\lambda})] = 0,$$

where $\mathbf{M}_a$ represents the adjoint magnetization as defined in the Theorem 1.

3. **Computation of the sensitivity of the problem:**

From the independence of the variables $\mathbf{p}$, $\mathbf{A}$ and $\boldsymbol{\lambda}$, in the definition of the Lagrangian function $\mathscr{L}$, and using the property of derivation under the integral, we obtain:

$$\frac{\partial \mathscr{L}(\mathbf{p}, \mathbf{A}, \boldsymbol{\lambda})}{\partial \mathrm{p}_i} = \int_\Omega \mu_0 \big[\boldsymbol{\lambda}.\frac{\partial \mathbf{J}(\mathbf{p})}{\partial \mathrm{p}_i} + \mathbf{B}(\boldsymbol{\lambda}).\frac{\partial \mathbf{M}(\mathbf{p})}{\partial \mathrm{p}_i} - \nu_0 \frac{\partial \nu_r(\mathbf{p})}{\partial \mathrm{p}_i} \mathbf{B}(\boldsymbol{\lambda}).\mathbf{B}(\mathbf{A})\big] d\Omega. \tag{17}$$

For each couple ($\mathbf{p}$,$\mathbf{A}$) satisfying constraint (3), we have $F_o(\mathbf{p}) = \mathscr{L}(\mathbf{p}, \mathbf{A(p)}, \boldsymbol{\lambda})$. Thus, using the chain rule theorem, we obtain:

$$\frac{\partial F_o(\mathbf{p})}{\partial \mathrm{p}_i} = \frac{\partial \mathscr{L}(\mathbf{p}, \mathbf{A}(\mathbf{p}), \boldsymbol{\lambda})}{\partial \mathrm{p}_i} + \frac{\partial \mathscr{L}(\mathbf{p}, \mathbf{A}(\mathbf{p}), \boldsymbol{\lambda})}{\partial \mathbf{A}}.\frac{\partial \mathbf{A}(\mathbf{p})}{\partial \mathrm{p}_i}. \tag{18}$$

Note that $\frac{\partial \mathscr{L}(\mathbf{p}, \mathbf{A}(\mathbf{p}), \boldsymbol{\lambda})}{\partial \mathbf{A}} = \mathbf{0}$ because of the stationarity of the Lagrangian function in $\mathbf{A}$, hence, we have:

$$\frac{\partial F_o(\mathbf{p})}{\partial \mathrm{p}_i} = \int_\Omega \mu_0 \big[\boldsymbol{\lambda}.\frac{\partial \mathbf{J}(\mathbf{p})}{\partial \mathrm{p}_i} + \mathbf{B}(\boldsymbol{\lambda}).\frac{\partial \mathbf{M}(\mathbf{p})}{\partial \mathrm{p}_i} - \nu_0 \frac{\partial \nu_r(\mathbf{p})}{\partial \mathrm{p}_i} \mathbf{B}(\boldsymbol{\lambda}).\mathbf{B}(\mathbf{A})\big] d\Omega$$

for each component p_i of $\mathbf{p}$.

□

From Theorem 1, we obtain directly (using the derivative with respect to $p_1 = \nu_r$) the following corollary:

Corollary 2. *The expression of the sensitivity with respect to ν is in 3D given by:*

$$\frac{\partial F_o(\nu_r)}{\partial \nu_r} = -\int_\Omega \boldsymbol{B}(\boldsymbol{\lambda}).\boldsymbol{B}(\boldsymbol{A})d\Omega. \tag{19}$$

Where $\boldsymbol{B}(\boldsymbol{\lambda})$ is obtained by solving the continuous adjoint problem provided by equation (10) *in Theorem 1.*

The weak formulation for those kind of 3D magnetostatic problem is:

$$\int_\Omega \nu \mathbf{B}(\mathbf{X}).\mathbf{B}(\boldsymbol{\varphi})d\Omega - \int_\Omega \mathbf{M}.\mathbf{B}(\boldsymbol{\varphi})d\Omega - \int_\Omega \mathbf{J}.\boldsymbol{\varphi}\, d\Omega = 0, \tag{20}$$

where $\boldsymbol{\varphi}$ is a test function of $\mathbf{H}_0(\mathbf{rot}, \Omega)$ to define the weak formulation in the finite element method.

Hence, by taking a simple magnetic circuit with only one coil, one ferromagnetic material part and no permanent magnet, we have to take $\mathbf{X} = \mathbf{A}$, $\mathbf{M} = \mathbf{0}$ and the only source is the current $\mathbf{J}$. Moreover, the adjoint problem is provided by taking $\mathbf{X} = \boldsymbol{\lambda}$, $\mathbf{J} = \mathbf{0}$ and the only source is now $\mathbf{M} = \mathbf{M}_a$.

It should be noticed that in the 3D case, it is necessary to add a gauge condition, in order to ensure the uniqueness of the solution using finite element method; this has to be done directly inside the 3D-finite element method solver.

4 Topology optimization algorithm

In Section 3, a way to compute efficiently the derivative of the function F_o is derived in Theorem 1 for 3D problems, these formulas are provided in continuous spaces. In this work, those formulas are solved numerically using finite element method. This involves discretization steps where the entire domain is discretized into small tetrahedral elements. The variables of the associated topology problem could be directly the tetrahedral elements in the variable domain Ω_V but they can also be defined by other cells, as for example hyperrectangles.

It remains a last difficulty. In some cases, the variables are discrete. Indeed, $p_1 = \nu_r$ represents the relative reluctivity in a point $(x, y, z)^T \in \Omega_V$. For a specific ferromagnetic material, p_1 can only takes two discrete values: $\nu_r = \nu_r^{\max} = \nu_0$ if we put air at $(x, y, z)^T$ or $\nu_r = \nu_r^{\min}$ if we put material at $(x, y, z)^T$. Note that, the other six parameters are continuous and can be directly used in a standard optimization code based on gradient descent steps.

In the next sub-section, the main method to deal with this issue is recalled. This is the well-known *SIMP* method (Bendsøe & Sigmund 2003, Bendsøe & Sigmund 1999, Sanogo & Messine 2018, Gauthey et al. 2021). In sub-section 4.2, our optimization code based on the *SIMP* method is provided and explained.

4.1 Penalization with material density method - SIMP

Focusing on the parameter p_1 which is discrete, we apply the *SIMP* method that is recalled in the following; for details see, (Sanogo & Messine 2018, Gauthey et al. 2021). This *SIMP* method could be applied in the same way on other parameters $p_i, i = 2 \cdots 7$ if necessary. Here, the other parameters $p_i, i = 2, \cdots, 7$ are fixed; note, that those remaining parameters are continuous and can be taken into account directly (without the use of SIMP) and hence, the main difficulty concerns the parameter p_1 which is discrete.

The discrete parameter p_1 is relaxed and becomes continuous between its two previous discrete values $p_1^{\min}$ and $p_1^{\max}$. This introduces composite materials between $p_1^{\min} = \nu_r^{\min}$ and $p_1^{\max} = \nu_r^{\max}$. This involves a magnetic structure which is generally not manufacturable. Hence, to prevent the appearance of these intermediate values, we penalize them introducing a density variable ρ belonging to [0,1] and linked to the design variable p_1 via a material interpolation scheme g such that, at a point x of Ω_V, one obtains: $g(\rho(x,y,z)) = p_1(x,y,z)$ with $g(0) = p_1^{\min} = \nu_r^{\min}$ and $g(1) = p_1^{\max} = \nu_r^{\max}$.

In the literature, there are several choices of interpolation functions g, that influences the final result of topology optimization, (Bendsøe & Sigmund 1999, Bendsøe & Sigmund 2003, Sanogo & Messine 2018, Gauthey et al. 2021, Lucchini et al. 2022). In this work, plenty penalization approaches were tested, however we present only results coming from the use of the polynomial interpolation scheme, as defined in (Bendsøe & Sigmund 1999):

$$p_1 = g(\rho) = p_1^{\min} + (p_1^{\max} - p_1^{\min})\rho^n, \tag{21}$$

where $n > 0$ is a penalty parameter. When the penalization parameter n is high, we enforce the solution to be discrete close to $p_1 \in \left\{p_1^{\min}, p_1^{\max}\right\}$. The main difficulty with this scheme is that it is not symmetrical and hence it favors materials with low values of ρ.

Therefore, the new variable of problem $(\mathcal{P})$ is now the material density ρ and then, using the chain rule theorem and from Theorem 1 in the case where $p_1 = \nu_r$, the new sensitivity with respect to ρ becomes:

$$\frac{\partial F_o}{\partial \rho} = -\int_\Omega \frac{\partial g}{\partial \rho}\mathbf{B}(\boldsymbol{\lambda}).\mathbf{B}(\mathbf{A})d\Omega \tag{22}$$

4.2 Optimization algorithm

In order to solve equation 22, the domain Ω_V is discretized into N cells Ω_{V_i}, each of which contains matter or not, according to the value of the density $\rho_i \in [0,1], i = 1, \cdots, N$ in Ω_{V_i}. Then, by denoting $\boldsymbol{\rho} = (\rho_1, \cdots, \rho_N)^T$, we can write the density variable ρ in all space as follows:

$$\rho = \sum_{i=1}^{N} \rho_i \mathbb{1}_{\Omega_{V_i}} + \rho_{\Omega\setminus\Omega_V}\mathbb{1}_{\Omega\setminus\Omega_V} \tag{23}$$

with $\rho_{\Omega\setminus\Omega_V}$ equals 1 in areas with ferromagnetic material and 0 in areas without ferromagnetic material outside the variable domain Ω_V.
Hence, using again the chain rule theorem and Theorem 1 in the case where $p_1 = \nu_r$, the sensitivity with respect to each element ρ_i of $\boldsymbol{\rho}$ becomes:

$$\frac{\partial F_o}{\partial \rho_i} = -\int_{\Omega_{V_i}} \frac{\partial g}{\partial \rho}\mathbf{B}(\boldsymbol{\lambda}).\mathbf{B}(\mathbf{A})d\Omega. \tag{24}$$

In order to solve problem $(\mathcal{P})$, the optimization algorithm needs the following information:

- The objective function and sensitivity calculation (see equation (24)).
- The constraints which are only the lower and upper bounds of the material density: $\boldsymbol{\rho} \in [0,1]^N$.
- The constraint imposed by the Maxwell equations is indirectly taken into account using the finite element method.

Our algorithm can be summarized in Fig. 1. Like any local optimization algorithm based on gradient descent, this optimization module starts from a *starting point* denoted by $\boldsymbol{\rho}^{[0]}$, build a sequence of points $\boldsymbol{\rho}^{[k]}$ and ends to $\boldsymbol{\rho}^{opt}$. Then, this point $\boldsymbol{\rho}^{opt}$ is analyzed because this solution is not necessarily discrete (does not belong necessarily to the set $\{0,1\}^N$). Hence, a test is added to check if $\boldsymbol{\rho}^{opt}$ is close to one of its two limits 0 or 1 with an imposed tolerance *tol*. If the tolerance *tol* is satisfied, the solution provided is $\boldsymbol{\rho}^{opt}$, otherwise the new starting point is updated by doing

$\boldsymbol{\rho}^{[0]} = \boldsymbol{\rho}^{opt}$) and by increasing the penalty parameter. This makes it possible to converge slowly but strongly to efficient design solutions. Indeed, by directly penalizing with a big parameter n, the optimization module converges to a local minimum which is very far from those obtained using our homotopy algorithm.

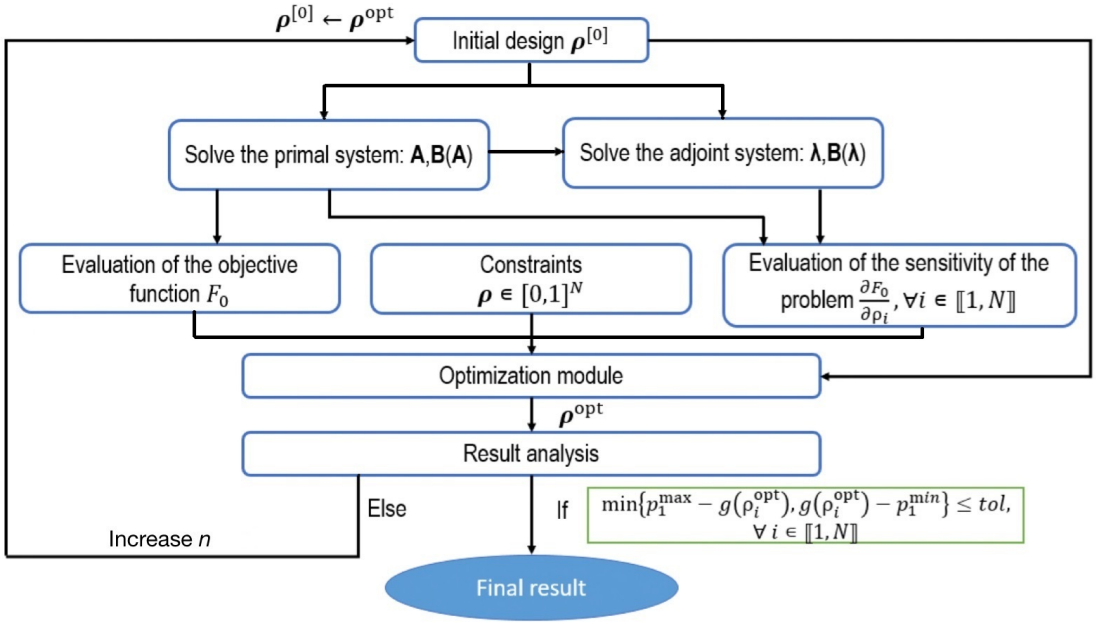

Figure 1: *SIMP* based topology optimization algorithm. (Source: figure created by authors)

4.3 Filtering technique

If we consider the expression of the derivative of F_o with respect to each element of $\boldsymbol{\rho}$, shown in equation (24), the final solution has generally *checkerboard patterns*, (Sigmund 2007). In order to make the solution more manufacturable, a regularization method must be added. Thus, in this work, a sensitivity filtering method has been used, (Sigmund 2007). The latter consists in modifying the values of the sensitivity of the cost function at each iteration through a spatial filter whose goal is to weight the value of the sensitivity in a target element by the value of its neighboring elements. In this work, several sensitivity filters have been tested, (Sigmund 2007, Sigmund & Maute 2013, Lucchini et al. 2022). For our problem the *bi-lateral sensitivity filter*, defined in (Sigmund 2007), provided the most efficient discrete solutions and so, the expression of the sensitivity with respect to an element *e* is replaced by:

$$\frac{\partial F_o}{\partial \rho_e} = \frac{\sum_{i \in N_e} w_{ie} \overline{w}(\frac{\partial F_o}{\partial \rho_i}) v_i \frac{\partial F_o}{\partial \rho_i}}{\sum_{i \in N_e} w_{ie} \overline{w}(\frac{\partial F_o}{\partial \rho_i}) v_i} \tag{25}$$

the sensibility weights are computed as follows:

$$\overline{w}(\frac{\partial F_o}{\partial \rho_i}) = \exp\left[-\frac{1}{2}\left(\frac{\frac{\partial F_o}{\partial \rho_i} - \frac{\partial F_o}{\partial \rho_e}}{\sigma_r}\right)^2\right] \text{ and } \sigma_r \in]0, 1].$$

Moreover, σ_r is fixed at 0.5, and the distance weighting w_{ie} is equal to $\max(0, r_{\min_e} - \text{dist}(i, e))$.

The following parameters are defined in this work such as:

- v_i is the volume of the element *i*.

- dist(i, e) is the distance between the center of the element *i* and the center of the element *e*.
- $r_{\min_e} = \delta h_e$; with $\delta \in \mathbb{R}_+^*$ and h_e is the greatest distance between the points constituting the element *e* (Euclidean norm of the difference between the coordinates of the most distant nodes of the element *e*).
- The set of neighbors of the element *e* is defined as follows: $N_e = \{i \mid \text{ dist}(i, e) \leq r_{\min_e}\}$.

Thus, in this section an efficient topology optimization algorithm based on adjoint methods and *SIMP* penalization technique is provided. Moreover, our methodology tends to provide more regularized solution close to manufacturable ones.

5 Numerical verifications on a 3D magnetic circuit

The aim of this section is to validate our methodology on a U-shaped magnetic circuit. This allows us to verify that the computation of the gradient based on our theoretical results (mainly Theorem 1 and Corollary 2) is close to the one obtained using the finite difference method. In a last sub-section, we address a design problem with a large number of variables (over 100,000 design variables).

5.1 Description of the design problems and numerical simulations

We consider here a simple magnetic circuit shown in Fig. 2 with one coil and two distinct variable zones which can be air or ferromagnetic materials. For this magnetic circuit, the design variable p_1 is the relative reluctivity ν_r which varies between the minimum value $p_1^{\min} = \nu_r^{\min} = 1/1000$ (corresponding to ferromagnetic material) and the maximum value $p_1^{\max} = \nu_r^{\max} = 1$ (corresponding to air).

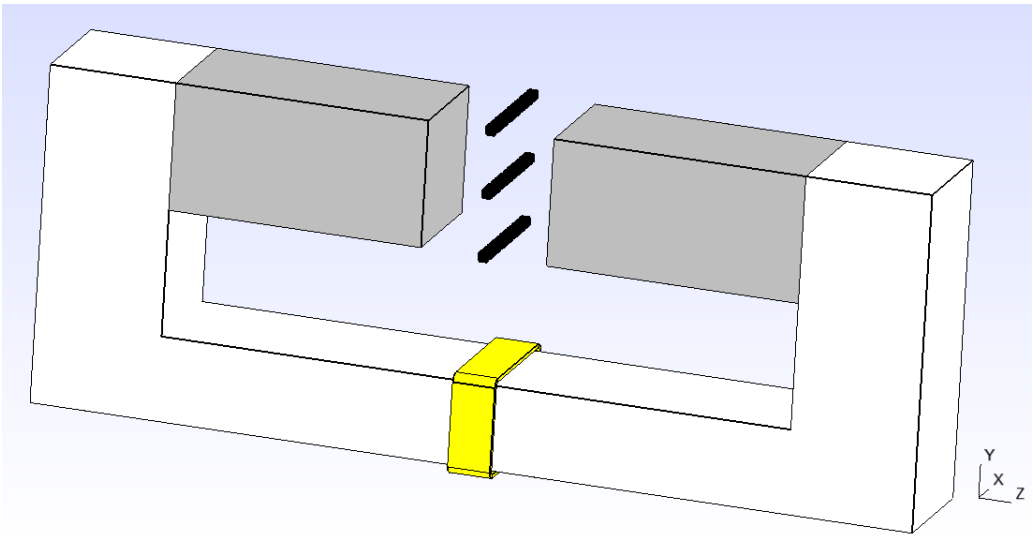

Figure 2: 3D magnetic circuit design problem. (Source: figure created by authors)

For this example, the magnetic circuit can be divided into 4 parts, as follows:

- A U-shaped ferromagnetic part which defines the fixed part of the magnetic circuit. It is represented in white on Fig. 2. Its dimensions are $105mm \times 40mm \times 15mm$, the thickness of the bottom hyperrectangle containing the coil is $10mm$ and the thickness of the both sides of the U-shaped circuit is $15mm$.
- A coil which is represented in yellow on Fig. 2. It is made up from 2 bottom and top bars of $15mm \times 0.4mm \times 5mm$ and 2 lateral bars of $10mm \times 0.4mm \times 5mm$ which are linked by 4 curved bars. This coil is crossed by a current density of $40A/mm^2$. This current density

is high for a real-life coil but the main idea here is to create a magnetic field in the target zone in order to validate our method whatever the origin of this field.

- Two design variable zones which are hyperrectangles of size $30mm \times 15mm \times 15mm$ which are represented in grey on Fig. 2. Each of these two parts is discretized into small variable cells that contain air or ferromagnetic material.
- One target zone which is represented in black on Fig. 2. It is bisected into small cubes of size $1mm$ into 3 lines, which are centered in the air gap between the two variable regions.

In order to solve the primal problem (3) and the adjoint problem (17), we use a finite element method solver which is `GetDP` software, (Dular & Geuzaine n.d.). To use `GetDP`, it is necessary to specify some elements of our problems: the Sobolev space, the weak formulation of the problem with the boundary conditions, the Jacobian and the type of numerical integration. `GetDP` is based on the mesher `Gmsh`, (Geuzaine & Remacle 2009, Remacle & Geuzaine n.d.) and the mesh of a domain owns some great importance because this involves the accuracy obtained on the solution versus the calculation time; so a previous study has been done to obtain efficiently a good accuracy on the solutions.

To solve intances based on this U-shape circuit, we can use two distinct meshes, as follows:

- *For the calculation of magnetic flux density:* we use a tetrahedral mesh in Ω. In order to ensure the accuracy of numerical values, this tetrahedral mesh is made on the whole study area Ω using `Gmsh` but is finer in Ω_T. Note that, a sufficiently accurate mesh has to be taken in all Ω in order to obtain a convergence on the computations of the flux density in Ω_T.
- *For the optimization cell variables:* we can discretize the variable area Ω_V (grey area on Fig. 2) into small hyperrectangle cells. Each cell represents a variable. Another possibility is to take the tetrahedral elements inside Ω_V, obtained from a finite element mesh, directly as variables.

Remark 1. *In order to validate the derivative, Ω_V is divided into 128 hyperectangles ($4 \times 4 \times 4$ in each side). This involves that the objective function F_o depends on 128 variables. Hence, the 128 partial derivatives based on our adjoint method were compared to those computed using a standard finite difference method for a material-filled configuration. The maximum value of the relative percentage difference between the two methods is less than 0.03%. We remark that the maximal errors are mainly concentrated in cell variables close to the corners of the hyperrectangles because the evaluation of the magnetic flux density is more difficult in these zones (even for fine meshes). Therefore, according to those numerical results, the continuous adjoint method as it is defined in Theorem 1 (without taking into account the* SIMP *penalization technique), is validated and thus, it can be used to provide efficient information about the gradient that will be used in topology optimization algorithms.*

Remark 2. *The adjoint method provides an adjoint problem which has the same difficulty to be solved than the primal problem (here the PDE Maxwell equation in magnetostatics). Thus, to perform the gradient of a function depending on N design variables by using a finite difference method, we need to solve $N + 1$ times the original PDE problem vs the resolution of 2 PDE problems for the adjoint method (the primal and the adjoint PDE problems). Note that using the adjoint method, the computation of the gradient is independent of the number of design variables.*

5.2 Design problem with a large number of variables

In this subsection, the goal is to solve problem $(\mathcal{P})$ on the magnetic circuit described in subsection 5.1 by considering a large number of design variables. In order to achieve that, the tetrahedrons of the finite element mesh in the variable zone Ω_V are taken as cell variables of the optimization design. This yields 106,801 design variables; note that the simulation problem owns 192,855 meshes, and remark that the variable region owns thinner meshes.

In this design example, the target magnetic flux density $\mathbf{B}_0$ is a field carried only along the z direction with a Gaussian shape according to the coordinate x:

$$\mathbf{B}_0 = \begin{pmatrix} 0 \\ 0 \\ B_{0z}(x) \end{pmatrix} = \begin{pmatrix} 0 \\ 0 \\ Ae^{-\frac{(x-x_0)^2}{2\sigma^2}} \end{pmatrix},$$

where $\sigma = 10^{-2}$ is the standard deviation of the Gaussian, $A = 4 \times 10^{-3}$ is a constant equal to the peak value of the Gaussian, and x_0 is the place in space where the peak is reached. Note that these kinds of imposed magnetic flux densities can be found in many applications, as for example for designing Hall effect thrusters, (Sanogo 2016, Sanogo & Messine 2018, Sanogo et al. 2014, Youness & Messine 2019*b*, Youness & Messine 2019*a*).

The choice of the penalty parameter n is very difficult because, if n is very large at the beginning, this leads to converge to a local minimum which will be not so interesting. Thus, we carry out a continuation process consisting in progressively increasing the penalization degree from $n = 1$ to $n = 100$. In this work, we take $n \in \{1, 2, 3, 4, 10, 20, 100\}$. Note that, for a fixed value of n the optimization module stops either if the maximum number of iterations 200 (400 for $n = 1$) is reached or if the stopping criteria is $\|\boldsymbol{\rho}^{[k+1]} - \boldsymbol{\rho}^{[k]}\|_\infty \leq 10^{-4}$ is satisfied.

In this paper, we choose to use the solver `MMA` (Method of Moving Asymptots), (Svanberg 1987); `MMA` is a nonlinear optimization code with a `MatLab` implemantation in opensource. `MMA` is a local search based algorithm and hence, a starting point has to be given. At each iteration of `MMA`, a convex approximation of the problem $(\mathcal{P})$ is computed. These approximations are mainly based on the gradients at the current iteration but also on some information of previous iterations. The approximated convex optimization problem is then solved and yields a unique optimal solution which becomes the new point at this iteration. Note that `MMA` can take into account constraints. Here, problem $(\mathcal{P})$ has only bound constraints.

Increasing the penalty degree n, makes it possible to enforce our method to converge slowly but with more trust to a very efficient (local) optimal design which is close to be manufacturable. In Table 1, we provide all the intermediate numerical results obtained at each disctinct steps of our homotopy algorithm (see Fig. 1). Note that the termination test is always the maximal number of iterations, providing so, optimized solution but not local optimal ones. We can remark that even if the values of the objective function decrease during the iterations, it is not the same for the number of intermediate values. Indeed, this number decreases until $n = 10$ and then increases a bit, see the fourth column of Table 1. Moreover, note that for the three optimizations, the final number of iterations is 1600 corresponding to a CPU-time of about 1 day of computations on a server (DELL server with 64GB of memory and with an `Intel(R) Xeon(R) Gold 5218R CPU` of 2.1GHz and 40 processors). We also note that the three optimizations carried out with or without the filter technique and using two distinct starting points lead to the same design solution with only a few pixels difference. The optimization without the filter brings the checkboarder effect into play, (Lucchini et al. 2022). Moreover, we also remark that the value of the objective function on the non-filtered solution is greater than the value of the filtered one. Hence, we think that this is due to the fact that using a filtering technique, the realizable domain is reduced and thus, in our design case, the optimization solver converges to a more interesting local minimum; i.e., it seems that without the use of a filtering technique, the algorithm stops too prematurely to a local minimum less interesting than the filtered one. In addition, we remark that on our design problem the starting point has not a big impact on the so obtained local solutions.

Thus, the best optimized design of the magnetic circuit, that we obtained so far, is presented in Fig. 3. This optimized design corresponds to the solution obtained at iteration 200 with the penalization parameter $n = 100$ when the starting point is full of air. Note that this solution is not close to be entirely discrete and several variables do not respect a tolerance about 5% of $p_1^{\min}$ and $p_1^{\max}$. Indeed, 11566 variables from 106801 are in $]p_1^{\min}$+5%,$p_1^{\max} - 5\%[$ which represents 10.8% of all the cell variables. Remark that those intermediate cell variables which have different

n	#its (=[k])	CPU-time			% intermediate densities $\nu_r \in]p_1^{\min}$+5%,$p_1^{\max} - 5\%[$			$F_o(\rho)$ ($\times 10^{-2}$)		
		Filt. air	Filt. full	No Filt. full	Filt. air	Filt. full	No Filt. full	Filt. air	Filt. full	No Filt. full
1	400	6h06	9h06	6h13	48.3%	32.9%	65.3%	19.6	4.59	4.37
2	200	3h03	4h06	3h00	30.3%	15.1%	18.6%	2.22	3.78	2.92
3	200	3h03	4h07	3h00	14.7%	10.3%	31.4%	1.62	2.81	2.34
4	200	3h03	3h35	3h00	7.34%	7.69%	7.80%	1.47	2.39	2.08
10	200	3h05	3h04	3h00	3.68%	3.34%	1.13%	1.36	2.08	2.10
20	200	3h05	3h04	3h00	4.63%	6.20%	1.01%	1.32	1.85	2.05
100	200	3h05	3h04	3h05	10.8%	12.4%	3.85%	1.28	1.58	2.19

Table 1: Numerical results using algorithm Fig. 1 to solve a 3D-design problem with over $100,000$ variables, for three optimizations: i) in blue, filter technique with a starting point corresponding to air everywhere; ii) in red, filter technique with a starting from a point corresponding to full material distribution; iii) in black, without using the filter technique with a starting point corresponding to full material distribution.

colors between blue (ferromagnetic material) and red (air) in Fig. 3 are in the border between the ferromagnetic material and air in the variable zone Ω_V. These difficulties are intrinsic in the use of *SIMP* approaches even if the penalization degree is high.

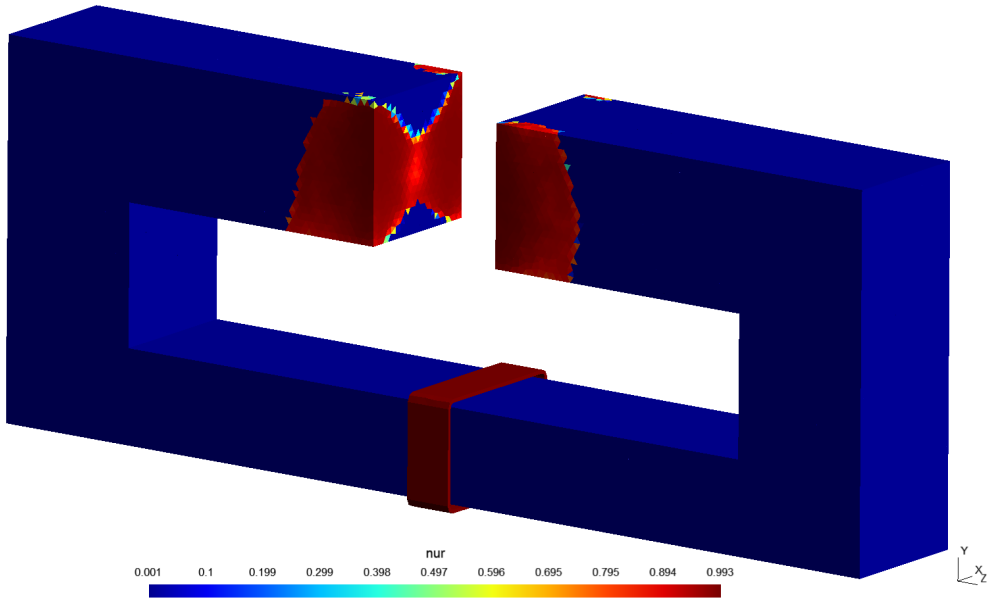

Figure 3: Topological optimization solution before post processing. (Source: figure created by authors)

Remark 3. *In order to obtain a circuit closer to be manufacturable, we could enforce the intermediate values of the reluctivity to be ferromagnetic material or air as follows: for* $\nu_r > \frac{\nu_r^{\max}+\nu_r^{\min}}{2}$ *we take* $\nu_r := \nu_r^{\max}$*, and for* $\nu_r < \frac{\nu_r^{\max}+\nu_r^{\min}}{2}$ *we take* $\nu_r := \nu_r^{\min}$.

Finally in Fig. 4, in Ω_T the reference magnetic flux density $\mathbf{B}_0$ and the magnetic flux density $\mathbf{B}$, computed from the best optimzed design, are plotted. Note that, $\mathbf{B}_1$,$\mathbf{B}_2$ and $\mathbf{B}_3$ correspond respectively to the magnetic flux density $\mathbf{B}$ at the three bars of the target area Ω_T from the bottom to the top, see Fig. 2.

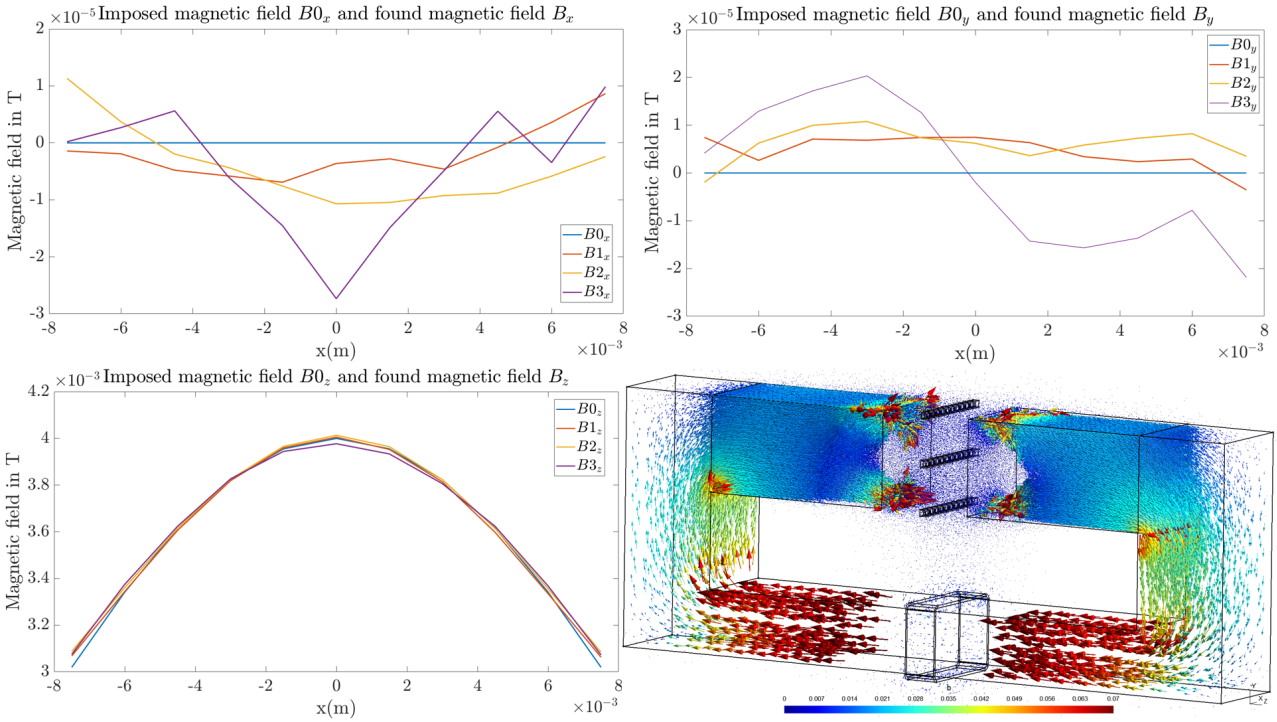

Figure 4: Comparison in Ω_T between the components of the imposed flux density $\mathbf{B}_0$ and the calculated flux density $\mathbf{B}$ in the three bars of Ω_T yielding the three density flux $\mathbf{B}_1, \mathbf{B}_2$ and $\mathbf{B}_3$, and a carthography of the flux density $\mathbf{B}$ of the solution design. (Source: figure created by authors)

In Fig. 4, it is shown that the components x and y of the flux density $\mathbf{B}$ are almost null (less than 10^{-5}) as asked. Moreover, note that the component z of $\mathbf{B}$ in the three bars are very close to the desired Gaussian function represented by the blue curve, see Fig. 4. These results shows that we are very close to obtain the asked flux density $\mathbf{B}_0$ and thus, that we are also close to a global optimal design solution with our best optimized design obtained so far.

6 Conclusion

In this paper, we have extended 2D-topology optimization methods in magnetostatics based on continuous adjoint and *SIMP* approches to the 3D case. Hence, some new theoretical results concerning efficient ways to compute derivative based on the adjoint method are provided for magnetostatic design problems in 3D. From this theorectical results, a quite new optimization algorithm is developed based on homotopy approaches to penalize more and more the continuous relaxation of the original discrete problem in order to enforce the convergence to a discrete solution (air or ferromagnetic material).

In a last part of the paper, numerical validations show that the gap between the gradients computed with adjoint method or with the finite difference technique is less than 0.03% for our design 3D problem in magnetostatics. Finally, our topology optimisation solver is efficiently used to solve a 3D-magnetic circuit design problem which owns up to 100,000 cell-variables.

It should be noticed that in 3D, simulation times and numerical efforts are much greater than for 2D resolutions. This limits the possibilities for numerical explorations in 3D. However, some extensions of this work could focus on developing this method to take into account the non-linearity of materials, the consideration of several physics (mechanical and magnetostatic) and other variable regions such as magnets or coils. Thus, the theory presented in this paper could be directly used to make a code capable of solving 3D multi-material design problems. Based on theoretical results in 2D, the non-linearity of materials and the consideration of mechanical constraints could be envisaged.

References

Aage, N., Andreassen, E., Lazarov, B. S. & Sigmund, O. (2017), 'Giga-voxel computational morphogenesis for structural design', *Nature* **550**(7674), 84–86.

Allaire, G. (2007), *Conception optimale de structures*, Springer, Berlin.

Allaire, G. & Alouges, F. (2015), *Polycopié du cours MAP 431: Analyse variationnelles des équations aux dérivées partielles*, École Polytechnique, Paris.

Bendsøe, M. P. & Sigmund, O. (1999), 'Material interpolation schemes in topology optimization', *Archive of applied mechanics* **69**, 635–654.

Bendsøe, M. P. & Sigmund, O. (2003), *Topology optimization: theory, methods, and applications*, Springer, Berlin.

Cherrière, T., Laurent, L., Hlioui, S., Louf, F., Duysinx, P., Geuzaine, C., Ben Ahmed, H., Gabsi, M. & Fernández, E. (2022), 'Multi-material topology optimization using wachspress interpolations for designing a 3-phase electrical machine stator', *Structural and Multidisciplinary Optimization* **65**(12), 352.

Dular, P. & Geuzaine, C. (n.d.), *GetDP reference manual*.
URL: *https://getdp.info/doc/texinfo/getdp.pdf*

Gangl, P. & Sturm, K. (2021), 'Asymptotic analysis and topological derivative for 3d quasi-linear magnetostatics', *ESAIM: Mathematical Modelling and Numerical Analysis* **55**, S853–S875.

Gauthey, T., Gangl, P. & Hassan, M. H. (2021), 'Multi-material topology optimization with continuous magnetization direction for permanent magnet synchronous reluctance motors', *arXiv preprint arXiv:2107.04825* .

Gauthey, T., Hassan, M. H., Messine, F. & Gillon, F. (2023), 'Topology optimization of the harmonic content for torque ripple minimization', *IEEE Transactions on Magnetics* pp. 1–4.

Geuzaine, C. & Remacle, J.-F. (2009), 'Gmsh: A 3-d finite element mesh generator with built-in pre-and post-processing facilities', *International journal for numerical methods in engineering* **79**(11), 1309–1331.

Lucchini, F., Torchio, R., Cirimele, V., Alotto, P. & Paolo, B. (2022), 'Topology optimization for electromagnetics: A survey', *IEEE Access* **10**, 98593–98611.

Masmoudi, M., Pommier, J. & Samet, B. (2005), 'The topological asymptotic expansion for the maxwell equations and some applications', *Inverse Problems* **21**(2), 547.

Remacle, J.-F. & Geuzaine, C. (n.d.), *Gmsh reference manual*.
URL: *https://gmsh.info/doc/texinfo/gmsh.pdf*

Sanogo, S. (2016), Conception optimale de circuits magnétiques dédiés à la propulsion spatiale électrique par des méthodes d'optimisation topologique, PhD thesis, Université Paul Sabatier-Toulouse III.

Sanogo, S. & Messine, F. (2018), 'Topology optimization in electromagnetism using simp method: Issues of material interpolation schemes', *COMPEL-The international journal for computation and mathematics in electrical and electronic engineering* **37**(6), 2138–2157.

Sanogo, S., Messine, F., Henaux, C. & Vilamot, R. (2014), 'Topology optimization for magnetic circuits dedicated to electric propulsion', *IEEE transactions on magnetics* **50**(12), 1–13.

Seebacher, P., Kaltenbacher, M., Wein, F. & Lehmann, H. (2021), 'A pseudo density topology optimization approach in nonlinear electromagnetism applied to a 3d actuator', *International Journal of Applied Electromagnetics and Mechanics* **65**(3), 545–559.

Sigmund, O. (2007), 'Morphology-based black and white filters for topology optimization', *Structural and Multidisciplinary Optimization* **33**, 401–424.

Sigmund, O. & Maute, K. (2013), 'Topology optimization approaches: A comparative review', *Structural and Multidisciplinary Optimization* **48**(6), 1031–1055.

Svanberg, K. (1987), 'The method of moving asymptotes—a new method for structural optimization', *International journal for numerical methods in engineering* **24**(2), 359–373.

Youness, R. & Messine, F. (2019*a*), Adjoint based topology optimization in nonlinear magnetostatics application to hall effect thrusters, *in* '2019 22nd International Conference on the Computation of Electromagnetic Fields (COMPUMAG)', IEEE, pp. 1–4.

Youness, R. & Messine, F. (2019*b*), 'An implementation of adjoint-based topology optimization in magnetostatics: Application to design hall-effect thrusters', *COMPEL-The international journal for computation and mathematics in electrical and electronic engineering* **38**(3), 1023–1035.